Inorganic Chemistry
Cite This: Inorg. Chem. 2019, 58, 5089−5095
Article
pubs.acs.org/IC

Water-Stable Europium 1,3,6,8-Tetrakis(4-carboxylphenyl)pyrene Framework for Efficient C_2H_2/CO_2 Separation

Rui Liu,[†] Qing-Yan Liu,*[,†] Rajamani Krishna,[‡] Wenjing Wang,[§] Chun-Ting He,[†] and Yu-Ling Wang*[,†]

[†]College of Chemistry and Chemical Engineering, Jiangxi Normal University, Nanchang, Jiangxi 330022, P. R. China
[‡]Van't Hoff Institute for Molecular Sciences, University of Amsterdam, Science Park 904, Amsterdam 1098 XH, The Netherlands
[§]State Key Laboratory of Structure Chemistry, Fujian Institute of Research on the Structure of Matter, Chinese Academy of Sciences, Fuzhou, Fujian 350002, P. R. China

Supporting Information

ABSTRACT: Compound $\{(Me_2NH_2)_3[Eu_7(\mu_3\text{-}O)_2(TBAPy)_5(H_2O)_6]\cdot 12.5DMF\}_n$ (**JXNU-5**), constructed from the 1,3,6,8-tetrakis(4-carboxylphenyl)pyrene ($TBAPy^{4-}$) ligand and one-dimensional (1D) europium carboxylate rods, is presented. **JXNU-5** has a three-dimensional framework with 1D channels. The strong coordination bonds between Eu^{III} ions with high charge densities and carboxylate O atoms as well as strong $\pi\cdots\pi$-stacking interactions between pyrenes lead to a water-resistant **JXNU-5**, which was verified by powder X-ray diffraction and surface area measurements. The breakthrough simulations and experiments demonstrate that an efficient C_2H_2/CO_2 (50/50 mixture) gas separation at ambient conditions was achieved with **JXNU-5**. The calculation results show that the dominating interactions between the absorbed C_2H_2 molecules and host framework are hydrogen bonds associated with the carboxylate O atoms exposed on the pores. Thus, an elegant example of a water-stable metal−organic framework for effective C_2H_2/CO_2 separation is demonstrated.

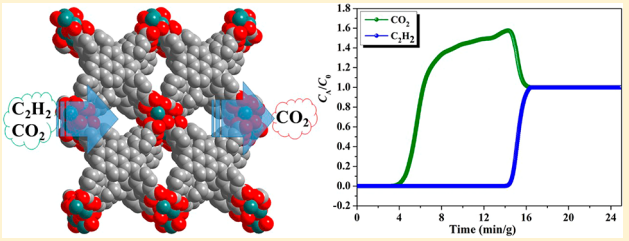

INTRODUCTION

Acetylene (C_2H_2) is the simplest alkyne and an important raw chemical for the preparation of a variety of fine chemicals including plastic, methyl acrylate, and vinyl derivatives, as well as electronic materials.[1] In addition, C_2H_2 is an important gas fuel for the production of oxyacetylene flame, which is widely used for welding and metal cutting. C_2H_2 is generated primarily by the oxidative coupling of methane in industry.[2] As a result, carbon dioxide (CO_2) is one of the byproducts in the process of oxidative coupling of methane to produce C_2H_2. Therefore, C_2H_2/CO_2 separation is an important industrial separation but a significant challenge because of the physicochemical similarities of C_2H_2 and CO_2. C_2H_2 and CO_2 both have linear molecular shapes ($3.32 \times 3.34 \times 5.7$ and $3.18 \times 3.33 \times 5.36$ Å^3 for C_2H_2 and CO_2, respectively) and similar boiling points [189.3 K (C_2H_2) and 194.7 K (CO_2)].[3]

Adsorption-based separation by porous solid materials is recognized as an energy-efficient and promising approach for industrial separation. As an important type of crystalline porous solid material, metal−organic frameworks (MOFs) are extensively investigated with respect to gas storage/separation,[4] catalysis,[5] proton conduction,[6] and drug delivery.[7] However, in view of their similarities, C_2H_2/CO_2 separations are only realized for a few MOFs.[8] Even so, claims of C_2H_2/CO_2 separation performance for most MOFs are solely supported by their single-component adsorption data. The breakthrough experiments based on a binary mixture,[9] which provides the actual separation performance of porous materials, are absent for most MOFs.

On the other hand, water or moisture is usually in the presence of an industrial process. Water-stable MOFs are desirable for industrial gas separations. Unfortunately, lots of MOFs lose their porosities upon exposure to water or moisture, which has limited their practical applications. For MOFs with crystalline structures and porosity, their water stability is usually verified by powder X-ray diffraction (PXRD) and surface area measurements. However, claims of water stability of a large number of MOFs are solely evidenced by their PXRD patterns. 1,3,6,8-Tetrakis(4-carboxylphenyl)-pyrene (H_4-TBAPy), with a central pyrene skeleton surrounded by four benzoate moieties, is expected to be an appropriate ligand for the construction of MOFs. The carboxylate O atoms and extensive π systems of the TBAPy-based MOFs may provide the preferential binding sites for the acidic H atoms of the C_2H_2 molecule, leading to promising candidates for C_2H_2/CO_2 separation. Herein, a three-dimensional (3D) structure, $\{(Me_2NH_2)_3[Eu_7(\mu_3\text{-}O)_2(TBAPy)_5(H_2O)_6]\cdot 12.5DMF\}_n$ (**JXNU-5**), constructed from the $TBAPy^{4-}$ ligand and the infinite one-dimensional

Received: January 18, 2019
Published: March 27, 2019

DOI: 10.1021/acs.inorgchem.9b00169
Inorg. Chem. 2019, 58, 5089−5095

(1D) europium carboxylate rods based on the linear trinuclear $Eu_3(COO)_6$ clusters and planar tetranuclear $Eu_4(\mu_3\text{-}O)_2$ clusters was synthesized and characterized. **JXNU-5** shows a high water stability, as evidenced by the PXRD and surface area measurements. The detailed gas sorption experiments, including breakthrough simulations and experiments, demonstrate that **JXNU-5** exhibits efficient C_2H_2/CO_2 separation performance.

EXPERIMENTAL SECTION

Gas Adsorption Measurements. N_2 (99.999%), C_2H_2 (99.999%), and CO_2 (99.999%) gases are used in the gas adsorption measurements. Gas adsorption was carried out in a Micromeritics ASAP2020 HD88 surface area analyzer. The as-prepared samples were exchanged with ethanol for 10 days. The exchanged samples were filtered and vacuumed at 25 °C for 4 h and then vacuumed under high vacuum at 85 °C for 28 h to give the guest-free framework (**JXNU-5a**).

Ideal Adsorbed Solution Theory (IAST) Calculations of the Adsorption Selectivity and Isosteric Heat of Adsorption. The IAST was applied to calculate the adsorption selectivity based on the experimental isotherm data of pure C_2H_2 and CO_2 fitted using a dual-site Langmuir model.[10] The adsorption selectivity for a binary mixture of components A and B is defined by

$$S_{ads} = \frac{q_A/q_B}{y_A/y_B}$$

where q_i represents the molar loading (mol kg^{-1}) at the adsorbed equilibrium of component *i*. y_i is the mole fraction in a bulk fluid mixture.

The isosteric heat of adsorption (Q_{st}) was calculated using the virial method[11] from fits of the adsorption isotherms at 273 and 298 K.

Breakthrough Simulations. The previous simulation methodology for transient breakthrough simulation was used here.[12] In the breakthrough simulations, the total bulk gas phase is 100 kPa and the temperature is 298 K. The partial pressures of both C_2H_2 and CO_2 are 50 kPa in the inlet feed gas mixture. The parameters for the breakthrough simulations are described in the Supporting Information. During a certain time interval, $\Delta\tau_{break}$, pure CO_2 (>99.95%) can be recovered in the gas phase.

Breakthrough Separation Experiments. The breakthrough separation experiments were measured on a homemade apparatus[13] for a 50/50 (v/v) C_2H_2/CO_2 mixture at 298 K and 1 atm. A stainless-steel column with a length of 120 mm and an inner diameter of 3 mm was used. A 0.46 g sample was packed into the adsorption column. Outlet gas from the column was monitored using a mass spectrometer (OmniStar, GSD 320 O1, Pfeiffer Vacuum) with a C-SEM/Faraday(M) detector (detection limit <50 ppm).

Synthesis of $\{(Me_2NH_2)_3[Eu_7(\mu_3\text{-}O)_2(TBAPy)_5(H_2O)_6]\cdot 12.5DMF\}_n$ (JXNU-5). $Eu(NO_3)_3\cdot 6H_2O$ (12 mg, 0.027 mmol), 1,3,6,8-tetrakis(*p*-benzoic acid)pyrene (17.2 mg, 0.025 mmol), 2-fluorobenzoic acid (17.5 mg, 0.125 mmol), and 0.3 mL of HNO_3 (3.5 M) were mixed with 3 mL of water and 3 mL of *N*,*N*-dimethylformamide (DMF), which was stirred at 30 °C for 0.5 h. The resulting mixture was transferred into a Parr Teflon-lined stainless-steel vessel, which was sealed and heated at 140 °C for 72 h. The pale-yellow crystals were washed with DMF to give **JXNU-5**. Yield: 13.2% based on $Eu(NO_3)_3\cdot 6H_2O$. Anal. Calcd for **JXNU-5** (5648.98): C, 56.02; N, 3.84; H, 4.16. Found: C, 56.11; N, 3.76; H, 4.11. IR spectrum (cm^{-1}): 3412 (w), 1660 (s), 1604 (s), 1585 (s), 1530 (s), 1413 (s), 1179 (w), 1101 (w), 1007 (w), 856 (w), 834 (w), 815 (w), 788 (m), 771 (w), 716 (m), 661 (w), 643 (w), 542 (w), 443 (w).

Structure Determination. X-ray diffraction data were collected on a Rigaku Oxford SuperNova diffractometer with Mo Kα radiation (λ = 0.71073 Å) and an EOS detector. Absorption correction and data reduction were conducted with the *CrysAlisPro* package.[14] The structure solution and refinement were established by *SHELXT*[15] and *SHELXTL*.[16] All atoms except for H atoms were refined with anisotropic thermal parameters. H atoms attached to C atoms were placed geometrically. Water H atoms are not located. Removal of the scattering of the disordered Me_2NH_2 cations and guest DMF molecules using the *SQUEEZE* tool of *PLATON* leads to a new set of solvent-free *hkl* reflections.[17] Table 1 lists the final refinement data. It should be noted that the Me_2NH_2 and guest DMF molecules are not included in the formula in the refinement data.

Table 1. Crystallographic Data for JXNU-5[a]

formula	$C_{220}H_{122}Eu_7O_{48}$
fw	4596.89
temp (K)	293(2)
cryst syst	triclinic
space group	$P\bar{1}$
Z	1
a (Å)	15.9745(8)
b (Å)	16.4434(6)
c (Å)	23.8952(11)
α (deg)	99.146(3)
β (deg)	108.266(4)
γ (deg)	90.310(3)
V (Å^3)	5874.4(5)
D_{calcd} (g cm^{-3})	1.299
μ (mm^{-1})	1.906
no. of reflns collected	65115
indep reflns	23968
obsd reflns [$I > 2\sigma(I)$]	17988
F(000)	2267
R_{int}	0.0530
R_1 [$I > 2\sigma(I)$]	0.0596
wR_2 (all data)	0.1516
CCDC	1891457

[a] $R_1 = \sum||F_o| - |F_c||/\sum|F_o|$ and $wR_2 = \{\sum[w(F_o^2 - F_c^2)^2]/\sum[w(F_o^2)^2]\}^{1/2}$.

RESULTS AND DISCUSSION

Crystal Structure. **JXNU-5** has a 3D framework based on 1D europium carboxylate rods featuring 1D channels. The Eu^{III} ions display different coordination geometries with coordination numbers of 8, 9, and 10. The Eu1 ion is located in an inversion center and 10-coordinated to 10 carboxylate O atoms from 6 $TBAPy^{4-}$ ligands (Figure S1). The Eu2 ion is nine-coordinated to eight carboxylate O atoms from six $TBAPy^{4-}$ ligands and one water molecule. Eu3 and Eu4 both have a coordination number of 8 but exhibit different coordination environments. The Eu3 ion is coordinated to seven carboxylate O atoms from six $TBAPy^{4-}$ ligands and one μ_3-O atom (Figure S1), while the Eu4 ion is eight-coordinated by four carboxylate O atoms from four $TBAPy^{4-}$ ligands, two μ_3-O atoms, and two water O atoms. The Eu–O bond distances vary from 2.322(4) to 2.894(5) Å (Table S1). As shown in Figure 1a, the Eu1, Eu2, and Eu2C atoms are bridged by the carboxylate groups to give a centrosymmetric linear trinuclear $Eu_3(COO)_6$ cluster with a Eu1···Eu2 separation of 4.04 Å. Four Eu atoms (Eu3, Eu3J, Eu4, and Eu4J) are linked by a pair of μ_3-O atoms to generate a centrosymmetric tetranuclear $Eu_4(\mu_3\text{-}O)_2(COO)_8$ cluster, wherein the four Eu···Eu edges are spanned by carboxylate groups. It was found that the four Eu atoms and two μ_3-O atoms are coplanar (Figure 1b), which is unusual because the two μ_3-O atoms usually serve as the capping atoms located above and below Ln_4 (Ln =

DOI: 10.1021/acs.inorgchem.9b00169
Inorg. Chem. 2019, 58, 5089−5095

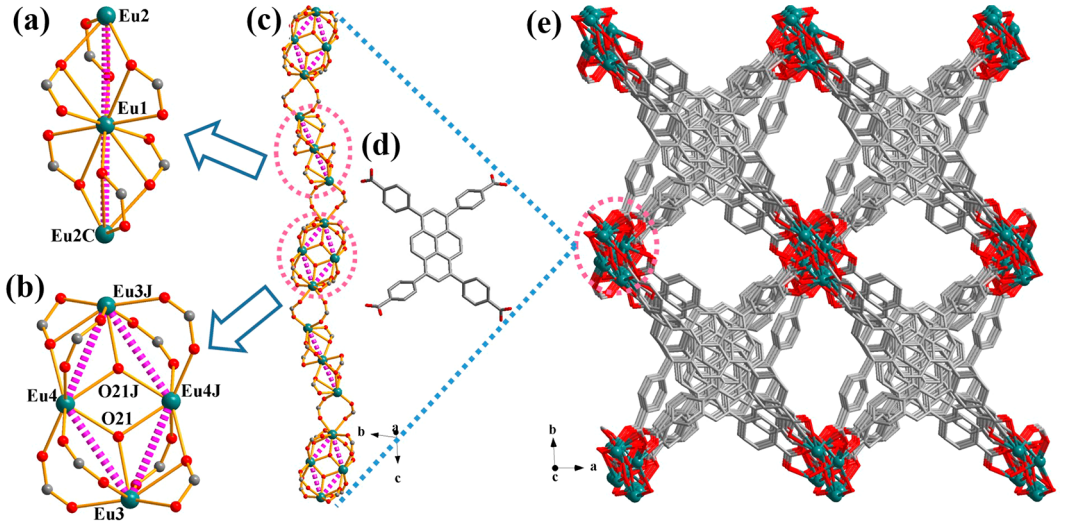

Figure 1. (a) Linear trinuclear cluster, (b) planar tetranuclear cluster, (c) 1D europium carboxylate rod, (d) organic ligand, and (e) 3D framework of **JNXU-5**.

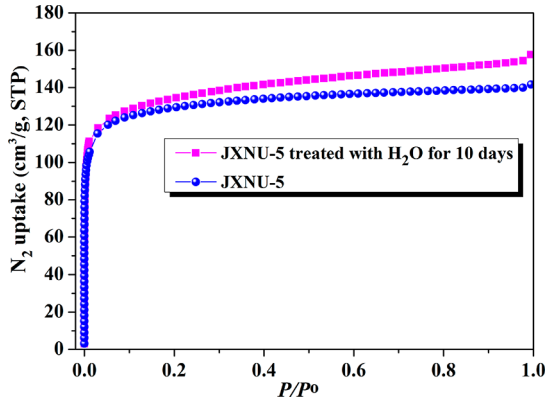

Figure 2. N_2 adsorption curves at 77 K for the as-synthesized **JXNU-5a** (close circles) and **JXNU-5a** after being immersed in water for 10 days (open squares).

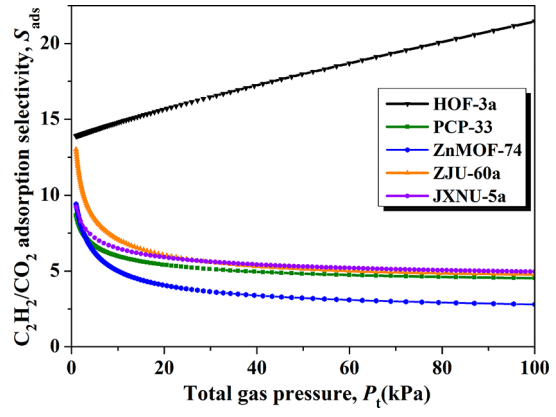

Figure 4. IAST calculations of the adsorption selectivities for a 50/50 C_2H_2/CO_2 mixture at 298 K for MOFs.

lanthanide) square in the reported $Ln_4(\mu_3\text{-}O)_2$ units.[18] The Eu3···Eu4, Eu3···Eu4J, and Eu4···Eu4J separations in the $Eu_4(\mu_3\text{-}O)_2$ cluster are 4.29, 3.98, and 3.96 Å, respectively. As depicted in Figure 1c, the linear trinuclear $Eu_3(COO)_6$ and tetranuclear $Eu_4(\mu_3\text{-}O)_2(COO)_8$ clusters are bridged by carboxylate groups to generate a 1D europium carboxylate rod extending to the *c* axis. The trinuclear $Eu_3(COO)_6$ and tetranuclear $Eu_4(\mu_3\text{-}O)_2(COO)_8$ clusters are alternately arranged in the 1D rod (Figure 1c). The 1D rodlike lanthanide carboxylates are commonly observed in the lanthanide compounds.[19] However, such a lanthanide carboxylate rod constructed from two types of different clusters are rarely observed. The three crystallographically independent $TBAPy^{4-}$

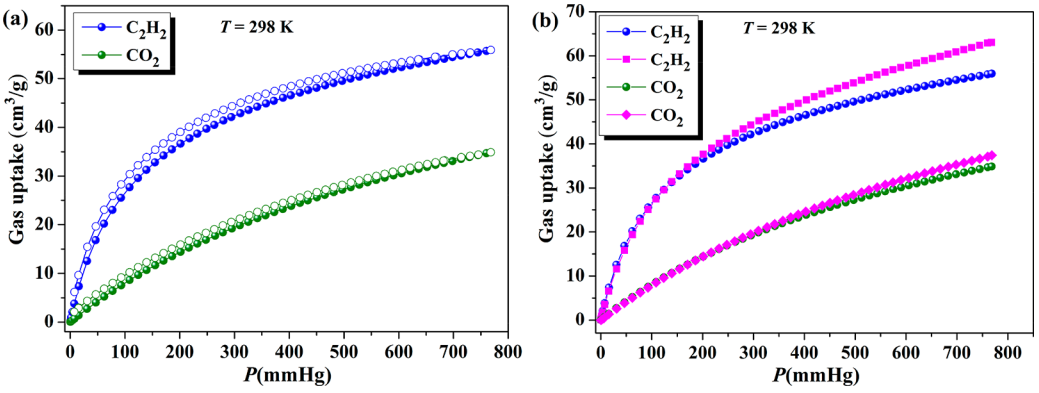

Figure 3. (a) C_2H_2 and CO_2 adsorption isotherms of **JXNU-5a** (adsorption, close circles; desorption, open circles). (b) C_2H_2 and CO_2 adsorption curves for **JXNU-5a** (circles) and **JXNU-5a** treated with water for 10 days (squares).

DOI: 10.1021/acs.inorgchem.9b00169
Inorg. Chem. 2019, 58, 5089−5095

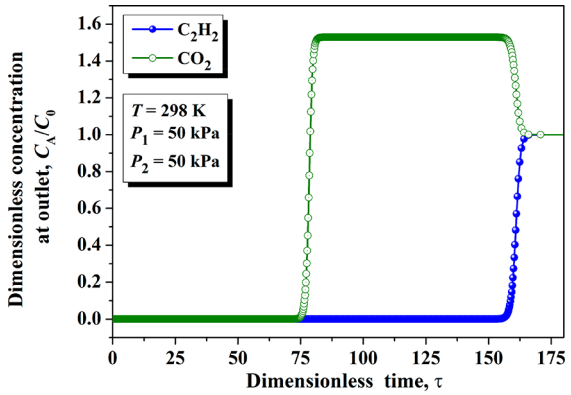

Figure 5. Simulated transient breakthrough curves for a 50/50 C_2H_2/CO_2 mixture at 100 kPa for **JXNU-5a** (C_A/C_0 = outlet concentration/feed concentration).

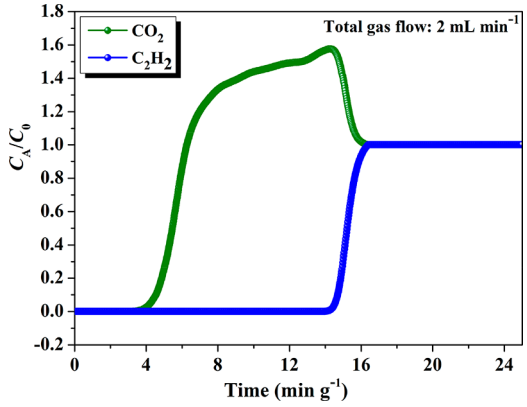

Figure 6. Experimental breakthrough curves for a 50/50 C_2H_2/CO_2 mixture for **JXNU-5a** at 298 K and 1 atm.

ligands adopt three coordination modes bridging seven or eight metal ions (Figure S2). As depicted in Figure 1e, each $TBAPy^{4-}$ ligand bridges four 1D europium carboxylate rods and links the 1D rods to give a 3D framework featuring 1D channels with an irregular aperture propagating along the *c* axis. The disordered DMF solvent molecules fill the channels and account for 31.2% of the volume of the unit cell.[17] The phase purity of the bulk materials was confirmed by PXRD (Figure S3). The results of thermogravimetric analysis (TGA) of **JXNU-5** show that the first weight loss occurred from 30 to 330 °C (Figure S4), which is the loss of all guest molecules and coordinated water molecules (weight loss: measured, 20.58%; theoretical, 20.51%). The TGA curve of the ethanol-exchanged **JXNU-5** sample indicates that the guest molecules can be removed from the framework below 90 °C. Thus, the ethanol-exchanged **JXNU-5** sample was evacuated under dynamic vacuum to give the activated sample of **JXNU-5a**.

Gas Adsorption Properties. The N_2 adsorption isotherm at 77 K for **JXNU-5a** shows a type I isotherm (Figures 2 and S5), indicating a microporous nature of the material. **JXNU-5a** takes up N_2 sharply at $P/P° < 0.01$ with a saturate amount of 141.5 cm^3 (STP) g^{-1} at 1 atm. The Brunauer–Emmett–Teller (BET) and Langmuir surface areas are 406 and 591 m^2 g^{-1} derived from the N_2 adsorption isotherm. The total pore volume of 0.22 cm^3 g^{-1} obtained from the N_2 adsorption experiment is close to the calculated one (0.24 cm^3 g^{-1}) from the crystal data. By analysis of the N_2 adsorption isotherm using the nonlocal density functional theory (NLDFT) model to give the narrow distribution of the micropores at 4.6 and 6.7 Å (Figure S5, inset). The PXRD patterns of the sample after adsorption and the pristine one are well-matched, indicating that the 3D framework is maintained during the adsorption process (Figure S3).

The porous nature of **JXNU-5a** encourages us to investigate its potential application in gas separation. The C_2H_2 and CO_2 adsorption isotherms have been collected on **JXNU-5a** at 273 and 298 K (Figures 3 and S6). Interestingly, **JXNU-5a** shows much different adsorption amounts for C_2H_2 and CO_2, indicating its potential for C_2H_2/CO_2 separation. At 273 K, the C_2H_2 and CO_2 adsorption amounts for **JXNU-5a** under 1 atm are 70.3 and 54.6 cm^3 g^{-1}, respectively. **JXNU-5a** takes up 55.9 and 34.8 cm^3 g^{-1} of C_2H_2 and CO_2 at 298 K and 1 atm (Figure 3a). The C_2H_2/CO_2 uptake ratio of 1.61 for **JXNU-5a** at 298 K is higher than those of Zn-MOF-74 (1.02 at 295 K),[20] FJU-22a (1.03 at 296 K),[9b] NKMOF-1-Ni (1.19 at 298 K),[9c] and UTSA-74a (1.52 at 298 K).[21] It is worth noting that the amount of absorbed C_2H_2 for **JXNU-5a** increases rapidly at low pressure, while CO_2 uptake nearly increases linearly with the pressure in the test pressure region (Figure 3). Such

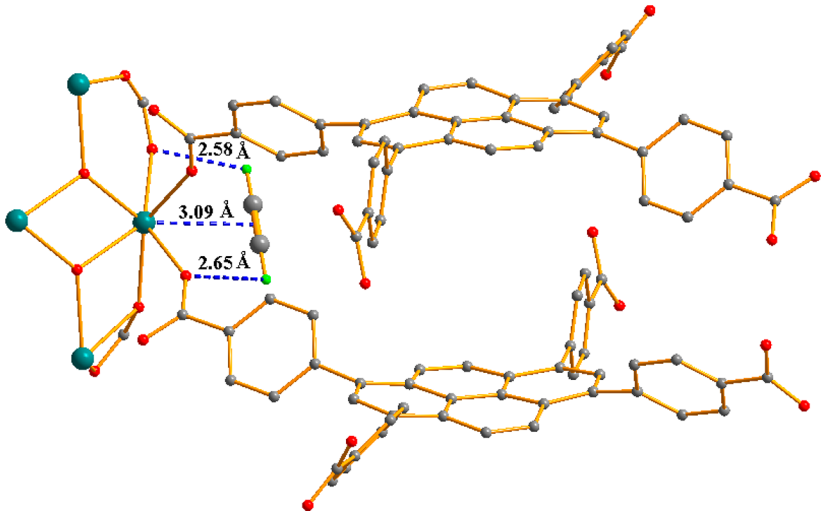

Figure 7. Favorable binding sites for C_2H_2 adsorption in **JXNU-5a**.

DOI: 10.1021/acs.inorgchem.9b00169
Inorg. Chem. 2019, 58, 5089–5095

different adsorption behaviors for C_2H_2 and CO_2 enable **JXNU-5a** to be a desirable material for C_2H_2/CO_2 separation. In view of the 3D structure (Figure 1e), plenty of carboxylate O atoms of the 1D europium carboxylate rods are exposed on the pore wall, which are desirable sites for the acidic H atoms of C_2H_2 molecules but are unfavorable sites for CO_2 molecules with two electronegative O atoms. Such a structural feature is favorable for C_2H_2/CO_2 separation.

To explore the feasibility of C_2H_2/CO_2 separation for **JXNU-5a**, the IAST calculation provided by Myers and Prausnitz[10] was conducted on the equimolar C_2H_2/CO_2 mixture. As depicted in Figure 4, at ambient pressure (100 kPa), the calculated adsorption selectivity (S_{ads}) for **JXNU-5a** is larger than those of ZJU-60a,[22] PCP-33,[23] and Zn-MOF-74,[20] while at low pressure, S_{ads} of **JXNU-5a** still exceeds those of PCP-33 and Zn-MOF-74 but is only slightly lower than that of ZJU-60a. Although HOF-3a displays the highest S_{ads} value among all of these MOFs,[24] its C_2H_2/CO_2 separation performance is significantly hampered by its very small BET surface area (165 $m^2\ g^{-1}$) and low C_2H_2 (47 $cm^3\ g^{-1}$) and CO_2 (21 $cm^3\ g^{-1}$) sorption capacities. The isosteric heat of adsorption Q_{st} at zero coverage fitted from the adsorption isotherms at 273 and 298 K are 32.9 and 25.2 kJ mol^{-1} for C_2H_2 and CO_2, respectively (Figures S7 and S8), which are comparable with those of UTSA-74a.[21]

Water Stability. To check the water stability, the freshly as-synthesized samples of **JXNU-5** were filtered and washed with DMF three times and then soaked in distilled water. After immersion in water for 10 days, the samples were filtered and dried under ambient conditions. The PXRD pattern of the sample treated with water is depicted in Figure S3, which shows that the diffraction peaks of the sample treated with water match well with those of the pristine sample. Thus, the **JXNU-5** material can maintain the crystallinity and structural integrity in aqueous solution. Furthermore, N_2 adsorption data at 77 K for the sample treated with water for 10 days were collected. The N_2 sorption curves of the pristine and water-treated samples overlap at the low-pressure region and display a slight disparity at high pressure (Figure 2), demonstrating **JXNU-5** with retention of the porosity after exposure to water. As shown in Figure 2, the saturated N_2 uptake for the water-treated sample is 154.3 cm^3 (STP) g^{-1}, which is slightly higher than that of the as-synthesized sample. The BET surface area of 425 $m^2\ g^{-1}$ for the water-treated sample is larger than that of the as-synthesized sample. Although the whole structural integrity and crystallinity of the compound after soaking in water were retained, few defects in the structure were generated. Such defects in the structure enhance the porosity, which is responsible for the larger N_2 uptake and surface area. Finally, the C_2H_2 and CO_2 adsorption data at 298 K for the samples soaked in water for 10 days were further measured. A slight difference was observed in the C_2H_2 and CO_2 adsorption curves for the as-synthesized and water-treated samples (Figure 3b). These results reveal that the gas adsorption performance of **JXNU-5a** was maintained after exposure to water.

Careful examination of the structure showed that the strong face-to-face $\pi\cdots\pi$ interactions between the central pyrenes in an offset fashion are observed in **JXNU-5** (Figure S9). Moreover, the coordination bonds between the trivalent Eu^{III} ions with high charge densities and carboxylate O atoms are much stronger than the coordination bonds between the divalent metal ions and carboxylate O atoms. Thus, the robust coordination bonds between the Ln ions and carboxylate O atoms and strong $\pi\cdots\pi$-stacking interactions between π-conjugated pyrenes account for the water-resistant ability of **JXNU-5**.

C_2H_2/CO_2 Separation. To evaluate the C_2H_2/CO_2 separation performance of **JXNU-5a**, transient breakthrough simulation was carried out using the established methodology by Krishna.[12] An equimolar C_2H_2/CO_2 mixture with a total pressure of 100 kPa was fed to a adsorption bed packed with the **JXNU-5a** sample at 298 K. As shown in Figure 5, CO_2 elutes first from the adsorption bed to give an effluent gas containing pure CO_2 until C_2H_2 starts to break through at a breakthrough time, τ_{break}. τ_{break} is defined as the time at which the concentration of C_2H_2 in the outlet gas is less than 500 ppm. For **JXNU-5a**, the τ_{break} value is 153, which leads to 1.54 mol L^{-1} of purified CO_2 (containing <500 ppm of C_2H_2) before the time τ_{break}. Such a result indicates that a clean C_2H_2/CO_2 separation can be realized at room temperature by the material of **JXNU-5a** (Figure 5).

The actual C_2H_2/CO_2 separation performance of **JXNU-5a** was established by the dynamic gas breakthrough experiments at 298 K and 1 atm with a 2 mL min^{-1} flow rate of a 50/50 (v/v) C_2H_2/CO_2 mixture. As depicted in Figure 6, CO_2 eluted through the packed column with the **JXNU-5a** solid first. C_2H_2 breakthrough occurred at 14.0 min g^{-1}. The C_2H_2 breakthrough time toward C_2H_2/CO_2 of **JXNU-5a** is shorter than the value of 19.1 min g^{-1} for FJU-22a[9b] and 35.1 min g^{-1} for NKMOF-1-Ni[9c] but longer than those of ZJU-196a (9.1 min g^{-1})[9d] and UTSA-300a (12 min g^{-1}).[25] It is notable that the concentration of C_2H_2 is below 50 ppm for the CO_2 outlet effluent before C_2H_2 breakthrough. The amount of captured C_2H_2 by the **JXNU-5a** material was calculated to be 726 mmol L^{-1} during the breakthrough process. Apparently, a complete separation of the C_2H_2/CO_2 mixtures was established with the **JXNU-5a** material. From the experimental breakthrough curves, the separation factor $\alpha = q_A y_B / q_B y_A$[26] is determined to be 9.9 for an equimolar C_2H_2/CO_2 mixture. The separation factor of **JXNU-5a** is larger than those of FJU-89a (3.0),[26b] HOF-3a (2.0),[24] and FJU-22a (1.9)[9b] but lower than the value of 20.1 for UTSA-74a[21] and 13 for DICRO-4-Ni-i.[27] Furthermore, the recycling experiments showed that the first- and second-cycle breakthrough curves are well-matched (Figure S10), indicating a good recyclability for C_2H_2/CO_2 separation. Thus, **JXNU-5a** exhibits a highly efficient separation performance toward the challenging C_2H_2/CO_2 mixture.

Finally, we performed grand canonical Monte Carlo (GCMC) simulations and dispersion-corrected density functional theory (DFT-D) calculations for understanding the adsorption behaviors of C_2H_2 and CO_2 in **JXNU-5a**. The calculated results show that the preferential adsorption sites for C_2H_2 and CO_2 are located at the channels nearby the 1D europium carboxylate rods. A C_2H_2 molecule forms strong hydrogen bonds with carboxylate O atoms with H···O distances of 2.58 and 2.65 Å (Figure 7). In addition, a weak M···π interaction between the open metal site (M) and the C_2H_2 molecule is also observed, while CO_2 only forms a weak interaction between the electronegative O atom and positively charged open metal site (Figure S11). Such distinct interactions between guest molecules and the host framework lead to an excellent C_2H_2/CO_2 separation performance.

DOI: 10.1021/acs.inorgchem.9b00169
Inorg. Chem. 2019, 58, 5089−5095

CONCLUSIONS

In summary, an europium carboxylate framework of **JXNU-5** with a large central pyrene skeleton ligand has been presented. **JXNU-5** with a porous structure shows a high water stability. An excellent C_2H_2/CO_2 separation performance for **JXNU-5a** has been established by both breakthrough simulations and experiments. The adsorbed C_2H_2 molecules were found to have interacted with the carboxylate O atoms of **JXNU-5a** through hydrogen bonds, while CO_2 molecules interact loosely with the framework of **JXNU-5a** through electrostatic dipole interactions. Thus, we demonstrate an elegant example of a water-resistant MOF for effective C_2H_2/CO_2 separation.

ASSOCIATED CONTENT

Supporting Information

The Supporting Information is available free of charge on the ACS Publications website at DOI: 10.1021/acs.inorgchem.9b00169.

Detailed experimental information, crystal structures, breakthrough simulations and experiments, PXRD patterns, TGA curves, Q_{st} of C_2H_2 and CO_2 adsorption, and GCMC and DFT calculations (PDF)

Accession Codes

CCDC 1891457 contains the supplementary crystallographic data for this paper. These data can be obtained free of charge via www.ccdc.cam.ac.uk/data_request/cif, or by emailing data_request@ccdc.cam.ac.uk, or by contacting The Cambridge Crystallographic Data Centre, 12 Union Road, Cambridge CB2 1EZ, UK; fax: +44 1223 336033.

AUTHOR INFORMATION

Corresponding Authors

*E-mail: qyliuchem@jxnu.edu.cn (Q.-Y.L.).
*E-mail:ylwang@jxnu.edu.cn (Y.-L.W.).

ORCID

Qing-Yan Liu: 0000-0003-1991-792X
Rajamani Krishna: 0000-0002-4784-8530
Yu-Ling Wang: 0000-0002-0839-699X

Notes

The authors declare no competing financial interest.

ACKNOWLEDGMENTS

We gratefully acknowledge the National Natural Science Foundation of China (Grants 21561015, 21661014, and 21861020) and Natural Science Foundation of Jiangxi Province (Grants 20181BAB203001 and 20171ACB20008) for financial support.

REFERENCES

(1) Pässler, P.; Hefner, W.; Buckl, K.; Meinass, H.; Wernicke, H. J.; Ebersberg, G.; Müller, R.; Bässler, J.; Behringer, H.; Mayer, D. *Ullmann's encyclopedia of industrial chemistry*; Wiley-VCH: Weinheim, Germany, 2000.

(2) Granada, A.; Karra, S. B.; Senkan, S. M. Conversion of methane into acetylene and ethylene by the chlorine-catalyzed oxidative-pyrolysis (CCOP) process. 1. oxidative pyrolysis of chloromethane. *Ind. Eng. Chem. Res.* **1987**, *26*, 1901−1905.

(3) Reid, C. R.; Thomas, K. M. Adsorption kinetics and size exclusion properties of probe molecules for the selective porosity in a carbon molecular sieve used for air separation. *J. Phys. Chem. B* **2001**, *105*, 10619−10629.

(4) (a) Moreau, F.; da Silva, I.; Al Smail, N. H.; Easun, T. L.; Savage, M.; Godfrey, H. G. W.; Parker, S. F.; Manuel, P.; Yang, S.; Schröder, M. Unravelling exceptional acetylene and carbon dioxide adsorption within a tetra-amide functionalized metal-organic framework. *Nat. Commun.* **2017**, *8*, 14085. (b) Taylor, M. K.; Runčevski, T.; Oktawiec, J.; Gonzalez, M. I.; Siegelman, R. L.; Mason, J. A.; Ye, J.; Brown, C. M.; Long, J. R. Tuning the adsorption-induced phase change in the flexible metal−organic framework Co(bdp). *J. Am. Chem. Soc.* **2016**, *138*, 15019−15026. (c) Qiu, S.; Xue, M.; Zhu, G. Metal−organic framework membranes: from synthesis to separation application. *Chem. Soc. Rev.* **2014**, *43*, 6116−6140. (d) Gelfand, B. S.; Huynh, R. P. S.; Mah, R. K.; Shimizu, G. K. H. Mediating order and modulating porosity by controlled hydrolysis in a phosphonate monoester metal−organic framework. *Angew. Chem., Int. Ed.* **2016**, *55*, 14614−14617. (e) Liang, C.-C.; Shi, Z.-L.; He, C.-T.; Tan, J.; Zhou, H.-D.; Zhou, H.-L.; Lee, Y.; Zhang, Y.-B. Engineering of pore geometry for ultrahigh capacity methane storage in mesoporous metal−organic frameworks. *J. Am. Chem. Soc.* **2017**, *139*, 13300−13303. (f) Liao, P.-Q.; Huang, N.-Y.; Zhang, W.-X.; Zhang, J.-P.; Chen, X.-M. Controlling guest conformation for efficient purification of butadiene. *Science* **2017**, *356*, 1193−1196. (g) Adil, K.; Belmabkhout, Y.; Pillai, R. S.; Cadiau, A.; Bhatt, P. M.; Assen, A. H.; Maurin, G.; Eddaoudi, M. Gas/vapour separation using ultra-microporous metal−organic frameworks: insights into the structure/separation relationship. *Chem. Soc. Rev.* **2017**, *46*, 3402. (h) Nugent, P.; Belmabkhout, Y.; Burd, S. D.; Cairns, A. J.; Luebke, R.; Forrest, K.; Pham, T.; Ma, S.; Space, B.; Wojtas, L.; Eddaoudi, M.; Zaworotko, M. J. Porous materials with optimal adsorption thermodynamics and kinetics for CO_2 separation. *Nature* **2013**, *495*, 80−84. (i) Lin, R.-B.; Li, L.; Zhou, H.-L.; Wu, H.; He, C.; Li, S.; Krishna, R.; Li, J.; Zhou, W.; Chen, B. Molecular sieving of ethylene from ethane using a rigid metal−organic framework. *Nat. Mater.* **2018**, *17*, 1128−1133. (j) Ye, Y.; Ma, Z.; Chen, L.; Lin, H.; Lin, Q.; Liu, L.; Li, Z.; Chen, S.; Zhang, Z.; Xiang, S. Microporous metal−organic frameworks with open metal sites and *p*-Lewis acidic pore surfaces for recovering ethylene from polyethylene off-gas. *J. Mater. Chem. A* **2018**, *6*, 20822−20828.

(5) (a) Zhu, Q.-L.; Li, J.; Xu, Q. Immobilizing metal nanoparticles to metal−organic frameworks with size and location control for optimizing catalytic performance. *J. Am. Chem. Soc.* **2013**, *135*, 10210−10213. (b) Li, B.; Leng, K.; Zhang, Y.; Dynes, J. J.; Wang, J.; Hu, Y.; Ma, D.; Shi, Z.; Zhu, L.; Zhang, D.; Sun, Y.; Chrzanowski, M.; Ma, S. Metal−organic framework based upon the synergy of a brønsted acid framework and lewis acid centers as a highly efficient heterogeneous catalyst for fixed-bed reactions. *J. Am. Chem. Soc.* **2015**, *137*, 4243−4248. (c) Noh, H.; Cui, Y.; Peters, A. W.; Pahls, D. R.; Ortuño, M. A.; Vermeulen, N. A.; Cramer, C. J.; Gagliardi, L.; Hupp, J. T.; Farha, O. K. An exceptionally stable metal−organic framework supported molybdenum (VI) oxide catalyst for cyclohexene epoxidation. *J. Am. Chem. Soc.* **2016**, *138*, 14720−14726. (d) Yoon, M.; Srirambalaji, R.; Kim, K. Homochiral metal−organic frameworks for asymmetric heterogeneous catalysis. *Chem. Rev.* **2012**, *112*, 1196−1231.

(6) (a) Sadakiyo, M.; Yamada, T.; Kitagawa, H. Rational designs for highly proton-conductive metal-organic frameworks. *J. Am. Chem. Soc.* **2009**, *131*, 9906−9907. (b) Taylor, J. M.; Dawson, K. W.; Shimizu, G. K. H. A water-stable metal−organic framework with highly acidic pores for proton-conducting applications. *J. Am. Chem. Soc.* **2013**, *135*, 1193−1196. (c) Zhou, L.-J.; Deng, W.-H.; Wang, Y.-L.; Xu, G.; Yin, S.-G.; Liu, Q.-Y. Lanthanide-potassium-biphenyl-3,3′- disulfonyl-4,4'-dicarboxylate frameworks: gas sorption, proton conductivity, and luminescent sensing of metal ions. *Inorg. Chem.* **2016**, *55*, 6271−6277. (d) Yang, F.; Xu, G.; Dou, Y.; Wang, B.; Zhang, H.; Wu, H.; Zhou, W.; Li, J.-R.; Chen, B. A flexible metal−organic framework with a high density of sulfonic acid sites for proton conduction. *Nat. Energy.* **2017**, *2*, 877−883. (e) Zhang, W.-W.; Wang, Y.-L.; Liu, Q.; Liu, Q.-Y. Lanthanide-benzophenone-3,3′-disulfonyl-4,4'-dicarboxylate frameworks: temperature and 1-hydroxypyren luminescence sensing, and proton conduction. *Inorg. Chem.* **2018**, *57*, 7805−7814.

DOI: 10.1021/acs.inorgchem.9b00169
Inorg. Chem. 2019, 58, 5089−5095

(7) (a) Zhao, X.; Mao, C.; Luong, K. T.; Lin, Q.; Zhai, Q.-G.; Feng, P.; Bu, X. Framework cationization by preemptive coordination of open metal sites for anion-exchange encapsulation of nucleotides and coenzymes. *Angew. Chem., Int. Ed.* **2016**, *55*, 2768−2772. (b) Dong, Z.; Sun, Y.; Chu, J.; Zhang, X.; Deng, H. Multivariate metal−organic frameworks for dialing-in the binding and programming the release of drug molecules. *J. Am. Chem. Soc.* **2017**, *139*, 14209−14216.

(8) (a) Matsuda, R.; Kitaura, R.; Kitagawa, S.; Kubota, Y.; Belosludov, R. V.; Kobayashi, T. C.; Sakamoto, H.; Chiba, T.; Takata, M.; Kawazoe, Y.; Mita, Y. Highly controlled acetylene accommodation in a metal−organic microporous material. *Nature* **2005**, *436*, 238−241. (b) Xu, H.; He, Y.; Zhang, Z.; Xiang, S.; Cai, J.; Cui, Y.; Yang, Y.; Qian, G.; Chen, B. A microporous metal−organic framework with both open metal and Lewis basic pyridyl sites for highly selective C_2H_2/CH_4 and C_2H_2/CO_2 gas separation at room temperature. *J. Mater. Chem. A* **2013**, *1*, 77−81. (c) Chang, G.; Li, B.; Wang, H.; Hu, T.; Bao, Z.; Chen, B. Control of interpenetration in a microporous metal−organic framework for significantly enhanced C_2H_2/CO_2 separation at room temperature. *Chem. Commun.* **2016**, *52*, 3494−3496. (d) Wen, H.-M.; Wang, H.; Li, B.; Cui, Y.; Wang, H.; Qian, G.; Chen, B. A microporous metal−organic framework with lewis basic nitrogen sites for high C_2H_2 storage and significantly enhanced C_2H_2/CO_2 separation at ambient conditions. *Inorg. Chem.* **2016**, *55*, 7214−7218.

(9) (a) Chen, K.-J.; Scott, H.-S.; Madden, D. G.; Pham, T.; Kumar, A.; Bajpai, A.; Lusi, M.; Forrest, K. A.; Space, B.; Perry, J. J., IV; Zaworotko, M. J. Benchmark C_2H_2/CO_2 and CO_2/C_2H_2 separation by two closely related hybrid ultramicroporous materials. *Chem.* **2016**, *1*, 753−765. (b) Yao, Z.; Zhang, Z.; Liu, L.; Li, Z.; Zhou, W.; Zhao, Y.; Han, Y.; Chen, B.; Krishna, R.; Xiang, S. Extraordinary separation of acetylene-containing mixtures with microporous metal−organic frameworks with open O donor sites and tunable robustness through control of the helical chain secondary building units. *Chem. - Eur. J.* **2016**, *22*, 5676−5683. (c) Peng, Y.-L.; Pham, T.; Li, P.; Wang, T.; Chen, Y.; Chen, K.-J.; Forrest, K. A.; Space, B.; Cheng, P.; Zaworotko, M. J.; Zhang, Z. Robust ultramicroporous metal−organic frameworks with benchmark affinity for acetylene. *Angew. Chem., Int. Ed.* **2018**, *57*, 10971−10975. (d) Zhang, L.; Jiang, K.; Li, L.; Xia, Y.-P.; Hu, T.-L.; Yang, Y.; Cui, Y.; Li, Bin; Chen, B.; Qian, G. Efficient separation of C_2H_2 from C_2H_2/CO_2 mixtures in an acid−base resistant metal−organic framework. *Chem. Commun.* **2018**, *54*, 4846−4849. (e) Li, L.; Wang, J.; Zhang, Z.; Yang, Q.; Yang, Y.; Su, B.; Bao, Z.; Ren, Q. Inverse adsorption separation of CO_2/C_2H_2 mixture in cyclodextrin-based metal−organic frameworks. *ACS Appl. Mater. Interfaces* **2019**, *11*, 2543−2550.

(10) Myers, A.-L.; Prausnitz, J. M. Thermodynamics of mixed-gas adsorption. *AIChE J.* **1965**, *11*, 121−127.

(11) Rowsell, J. L. C.; Yaghi, O. M. Effects of Functionalization, Catenation, and Variation of the Metal Oxide and Organic Linking Units on the Low-Pressure Hydrogen Adsorption Properties of Metal−Organic Frameworks. *J. Am. Chem. Soc.* **2006**, *128*, 1304−1315.

(12) (a) Krishna, R. The maxwell-stefan description of mixture diffusion in nanoporous crystalline materials. *Microporous Mesoporous Mater.* **2014**, *185*, 30−50. (b) Krishna, R. Methodologies for Evaluation of Metal-organic frameworks in separation applications. *RSC Adv.* **2015**, *5*, 52269−52295.

(13) Wang, H.-H.; Liu, Q.-Y.; Li, L.; Krishna, R.; Wang, Y.-L.; Peng, X.-W.; He, C.-T.; Lin, R.-B.; Chen, B. A Nickel-4'-(3,5-Dicarboxyphenyl)-2,2',6',2''-terpyridine Framework: Efficient Separation of Ethylene from Acetylene/Ethylene Mixtures with a High Productivity. *Inorg. Chem.* **2018**, *57*, 9489−9494.

(14) *CrysAlisPro*; Rigaku Oxford Diffraction: The Woodlands, TX, 2015.

(15) Sheldrick, G. M. SHELXT−integrated space-group and crystal-structure determination. *Acta Crystallogr., Sect. A: Found. Adv.* **2015**, *A71*, 3−8.

(16) Sheldrick, G. M. Crystal structure efinement with SHELXL. *Acta Crystallogr.* **2015**, *C71*, 3−8.

(17) Spek, A. L. *PLATON: A multipurpose Crystallographic Tool*; Utrecht University: Utrecht, The Netherlands, 2001.

(18) (a) Feng, W.; Zhang, Y.; Zhang, Z.; Lü, X.; Liu, H.; Shi, G.; Zou, D.; Song, J.; Fan, D.; Wong, W.-K.; Jones, R. A. Anion-induced self-assembly of luminescent and magnetic homoleptic cyclic tetranuclear $Ln_4(Salen)_4$ and $Ln_4(Salen)_2$ complexes (Ln = Nd, Yb, Er, or Gd). *Inorg. Chem.* **2012**, *51*, 11377−11386. (b) Chakraborty, A.; Bag, P.; Goura, J.; Bar, A.-K.; Sutter, J.-P.; Chandrasekhar, V. Chair-shaped $Mn^{II}_2Ln^{III}_4$ (Ln = Gd, Tb, Dy, Ho) heterometallic complexes assembled from a tricompartmental aminobenzohydrazide ligand. *Cryst. Growth Des.* **2015**, *15*, 848−857.

(19) (a) Guo, X.; Zhu, G.; Sun, F.; Li, Z.; Zhao, X.; Li, X.; Wang, H.; Qiu, S. Synthesis, Structure, and Luminescent Properties of Microporous Lanthanide Metal−Organic Frameworks with Inorganic Rod-Shaped Building Units. *Inorg. Chem.* **2006**, *45*, 2581−2587. (b) Liu, Q.-Y.; Li, Y.-L.; Wang, Y.-L.; Liu, C.-M.; Ding, L.-W.; Liu, Y. Ionothermal syntheses of a 3D dysprosium−1,4-benzenedicarboxylate framework based on the 1D rod-shaped dysprosium−carboxylate building blocks exhibiting slow magnetization relaxation. *CrystEngComm* **2014**, *16*, 486−491. (c) Wang, Y.-L.; Jiang, Y.-L.; Xiahou, Z.-J.; Fu, J.-H.; Liu, Q.-Y. Diversity of Lanthanide(III)- 2,5-Dihydroxy-1,4-benzenedicarboxylate Extended Frameworks: Syntheses, Structures, and Magnetic Properties. *Dalton Trans.* **2012**, *41*, 11428−11437.

(20) (a) Caskey, S. R.; Wong-Foy, A. G.; Matzger, A. J. Dramatic tuning of carbon dioxide uptake via metal substitution in a coordination polymer with cylindrical pores. *J. Am. Chem. Soc.* **2008**, *130*, 10870−10871. (b) Xiang, S.; Zhou, W.; Zhang, Z.; Green, M. A.; Liu, Y.; Chen, B. Open metal sites within isostructural metal−organic frameworks for differential recognition of acetylene and extraordinarily high acetylene storage capacity at room temperature. *Angew. Chem., Int. Ed.* **2010**, *49*, 4615−4618.

(21) Luo, F.; Yan, C.; Dang, L.; Krishna, R.; Zhou, W.; Wu, H.; Dong, X.; Han, Y.; Hu, T.-L.; O'Keeffe, M.; Wang, L.; Luo, M.; Lin, R.-B.; Chen, B. UTSA-74: A MOF-74 isomer with two accessible binding sites per metal center for highly selective gas separation. *J. Am. Chem. Soc.* **2016**, *138*, 5678−5684.

(22) Duan, X.; Zhang, Q.; Cai, J.; Yang, Y.; Cui, Y.; He, Y.; Wu, C.; Krishna, R.; Chen, B.; Qian, G. A new metal−organic framework with potential for adsorptive separation of methane from carbon dioxide, acetylene, ethylene, and ethane established by simulated breakthrough experiments. *J. Mater. Chem. A* **2014**, *2*, 2628−2633.

(23) Duan, J.; Jin, W.; Krishna, R. Natural gas purification using a porous coordination polymer with water and chemical stability. *Inorg. Chem.* **2015**, *54*, 4279−4284.

(24) Li, P.; He, Y.; Zhao, Y.; Weng, L.; Wang, H.; Krishna, R.; Wu, H.; Zhou, W.; O'Keeffe, M.; Han, Y.; Chen, B. A rod-packing microporous hydrogen-bonded organic framework for highly selective separation of C_2H_2/CO_2 at room temperature. *Angew. Chem., Int. Ed.* **2014**, *54*, 574−577.

(25) Lin, R.-B.; Li, L.; Wu, H.; Arman, H.; Li, B.; Lin, R.-G.; Zhou, W.; Chen, B. Optimized Separation of Acetylene from Carbon Dioxide and Ethylene in a Microporous Material. *J. Am. Chem. Soc.* **2017**, *139*, 8022−8028.

(26) (a) Liu, J.; Tian, J.; Thallapally, P. K.; McGrail, B. P. Selective CO_2 Capture from Flue Gas Using Metal-Organic Frameworks-A Fixed Bed Study. *J. Phys. Chem. C* **2012**, *116*, 9575−9581. (b) Ye, Y.; Chen, S.; Chen, L.; Huang, J.; Ma, Z.; Li, Z.; Yao, Z.; Zhang, J.; Zhang, Z.; Xiang, S. Additive-induced supramolecular isomerism and enhancement of robustness in Co(II) based MOFs for efficiently trapping acetylene from acetylene-containing mixtures. *ACS Appl. Mater. Interfaces* **2018**, *10*, 30912−30918.

(27) Scott, H. S.; Shivanna, M.; Bajpai, A.; Madden, D. G.; Chen, K.-J.; Pham, T.; Forrest, K. A.; Hogan, A.; Space, B.; Perry, J. J., IV; Zaworotko, M. J. Highly Selective Separation of C_2H_2 from CO_2 by a New Dichromate-Based Hybrid Ultramicroporous Material. *ACS Appl. Mater. Interfaces* **2017**, *9*, 33395−33400.

DOI: 10.1021/acs.inorgchem.9b00169
Inorg. Chem. 2019, 58, 5089−5095

Water-stable Europium-1,3,6,8-tetrakis(4-carboxylphenyl)pyrene Framework for Efficient C_2H_2/CO_2 Separation

Rui Liu,[†] Qing-Yan Liu *,[†] Rajamani Krishna,[‡] Wenjing Wang,[§] Chun-Ting He,[†] and Yu-Ling Wang *,[†]

[†]*College of Chemistry and Chemical Engineering, Jiangxi Normal University, Nanchang 330022, P. R. China*

[‡] *Van't Hoff Institute for Molecular Sciences, University of Amsterdam, Science Park 904, 1098 XH Amsterdam, The Netherlands*

[§]*State Key Laboratory of Structure Chemistry, Fujian Institute of Research on the Structure of Matter, Chinese Academy of Sciences, Fuzhou, Fujian 350002, P. R. China*

Supporting Information

Experimental Section

Chemicals. All chemicals were purchased commercially.

Physical Measurements. FT-IR spectrum was recorded from KBr disc on a Perkin-Elmer Spectrum One FT-IR spectrometer ranging from 400 to 4000 cm^{-1}. Thermogravimetric analyses were performed under a nitrogen atmosphere with a heating rate of 10 °C/min using a PE Diamond thermogravimetric analyser. Powder X-ray diffraction analyses were performed on a Rigaku Dmax2500 diffractometer with Cu-Kα radiation (λ = 1.5418 Å).

Ideal adsorbed solution theory (IAST) calculations of adsorption selectivity and isosteric heat of adsorption. The IAST was used to predict mixed gas behavior from experimentally measured single-component isotherms.[1] The experimentally measured loadings for C_2H_2 and CO_2 at 298 K in **JXNU-5a** were fitted with the dual-site Langmuir isotherm model.

$$q = q_{A,sat}\frac{b_A p}{1+b_A p} + q_{B,sat}\frac{b_B p}{1+b_B p}$$

Where p (unit: kPa) is the pressure of the bulk gas at equilibrium with the adsorbed phase, q (unit: mol kg^{-1}) is the adsorbed amount per mass of adsorbent, $q_{A,sat}$ and $q_{B,sat}$ (unit: mmol g^{-1}) are the saturation capacities of two different sites, b_A and b_B (unit: 1/kPa) are the affinity coefficients of these sites. The Langmuir parameters for each site is temperature-dependent.

$$b_A = b_{A0}\exp\left(\frac{E_A}{RT}\right); \quad b_b = b_{B0}\exp\left(\frac{E_B}{RT}\right)$$

The fitting parameters of dual-site Langmuir isotherm model are provided in Table S2. The adsorption selectivity for binary mixture (A and B) using the Langmuir fitting parameters is defined by

$$S_{ads} = \frac{q_A/q_B}{y_A/y_B}$$

(where the q_A and q_B represent the molar loadings (mol kg^{-1}). The y_A and y_B ($y_B = 1 - y_A$) are the mole fractions in a bulk fluid mixture.).

The isosteric heat of adsorption, Q_{st}, is defined as

$$Q_{st} = RT^2\left(\frac{\partial \ln p}{\partial T}\right)_q$$

The C_2H_2 and CO_2 adsorption data were fitted using a Virial-type expression (Figure S7). [2] Then the Q_{st} values for C_2H_2 and CO_2 are calculated based on the fitting parameters with the above expression.

Transient breakthrough simulations. The performance of industrial fixed bed adsorber is dictated by a combination of adsorption selectivity and uptake capacity. We perform transient breakthrough simulations using the simulation methodology described in the literature.[3,4] For the breakthrough simulations, the following parameter values were used: length of packed bed, L = 0.3 m; voidage of packed bed, ε = 0.4; superficial gas velocity at inlet, u = 0.04 m/s. The transient breakthrough simulation results are presented in terms of a *dimensionless* time, τ, defined as $\tau = \frac{tu}{\varepsilon L}$.

During the initial transience, the effluent gas contains pure CO_2 and this continues until C_2H_2 starts breaking through because its uptake capacity in the MOF has been reached.

During a certain time interval, $\Delta\tau$, pure CO_2 can be recovered in the gas phase. We set the purity

of CO_2 to 99.95%. The MOFs are all compared on the basis of the moles of 99.95% pure CO_2 produced per L of adsorbent material.

Breakthrough experiments. The breakthrough separation experiments were measured on a homemade apparatus for C_2H_2/CO_2 (v/v = 50/50) mixture at 298 K and 1 atm. The stainless steel column with a length of 120 mm and an inner diameter of 3 mm was used. 0.46 g sample was packed into the adsorption column. The column was placed in a temperature-controlled environment (298 K). The mixed gas flow rate during the breakthrough process is 2 mL min^{-1} of a C_2H_2/CO_2 (v:v =50:50) at 1 atm. Outlet gas from the column was monitored using a mass spectrometer (OmniStar, GSD 320 O1, Pfeiffer vacuum) with a C-SEM/Faraday(M) detector (detection limit < 50 ppm). From the experimental breakthrough curves, the separation factor defined by $\alpha = (q_A y_B)/ (q_B y_A)$,[5] can be determined ($q_i$ is the equilibrium adsorption capacity of gas i (mmol g^{-1}) and y_i is the molar fraction of gas i (i = A, B) in the gas mixture). On the basis of the mass balance, the gas adsorption capacity (q_i) can be determined as follows: [5]

$$q_i = \frac{C_i V}{22.4 \times m} \times \int_0^t \left(1 - \frac{F}{F_0}\right) dt$$

Where q_i is the equilibrium adsorption capacity of gas i (mmol g^{-1}), C_i is the feed gas concentration, V is the volumetric feed flow rate (cm^3 min^{-1}), t is the adsorption time (min), F_0 and F are the inlet and outlet gas molar flow rates, respectively, and m is the mass of the adsorbent (g).

Sample information in breakthrough experiment:

Length of adsorption bed:	L = 120 mm
Inner diameter of adsorption bed:	φ = 3 mm
Total flow:	2 mL/min
Temperature:	298 K
Total pressure:	1 atm
weight of MOF sample	0.46 g

Grand canonical Monte Carlo (GCMC) simulation and Density Functional Theory (DFT) Calculation. All the GCMC simulation was performed using the Materials Studio 5.5 package. The adsorption sites of C_2H_2 and CO_2 at 298 K were obtained from GCMC simulations through the fixed

loading task in the Sorption module. The host framework and the guest molecules were both regarded as rigid. The simulation box consisted of eight unit cell and the Metropolis method based on the universal forcefield (UFF) was used. The Q_{Eq} derived charges and the ESP charges derived by DFT were employed to the host framework and guest atoms, respectively. The cutoff radius was chosen as 15.5 Å for the Lennard-Jones (LJ) potential, and the equilibration steps and production steps were both set as 5×10^6. We first optimized the **JXNU-5a** structure using the DFT method with periodic boundary. The widely used generalized gradient approximation (GGA) with the Perdew-Burke-Ernzerhof (PBE) functional and the double numerical plus d-functions (DND) basis set were used. An accurate DFT Semi-core Pseudopots (DSPP) was employed for the metal atoms. For all the DFT calculations, the energy, gradient and displacement convergence criterions were set as 1×10^{-5} Ha, 2×10^{-3} Å and 5×10^{-3} Å, respectively.

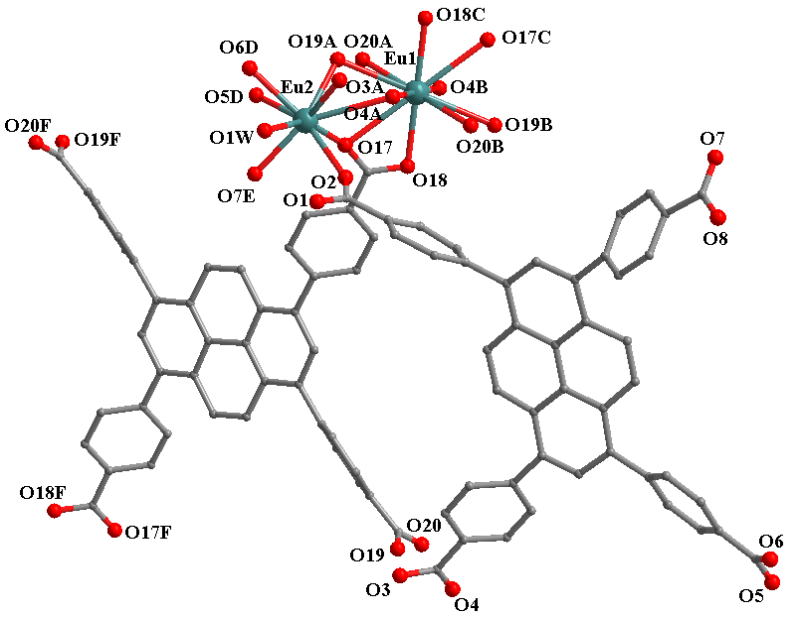

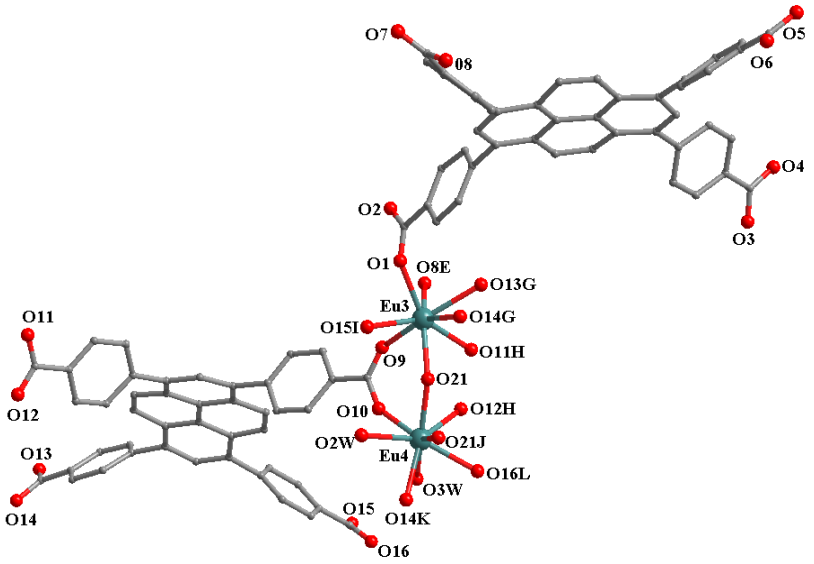

Figure S1. The coordination environments of the Eu(III) ions in **JXNU-5**.(Symmetry codes: A $x-1$, y , z; B $2-x$, $1-y$, $2-z$; C $1-x$, $1-y$, $2-z$; D $x-1$, $1+y$, z; E x, $1+y$, z; F $2-x$, $2-y$, $2-z$; G $1+x$, $y-1$, z; H $1+x$, y, z; I x, $y-1$, z; J $1-x$, $1-y$, $1-z$; K $-x$, $2-y$, $1-z$; L $1-x$, $2-y$, $1-z$.)

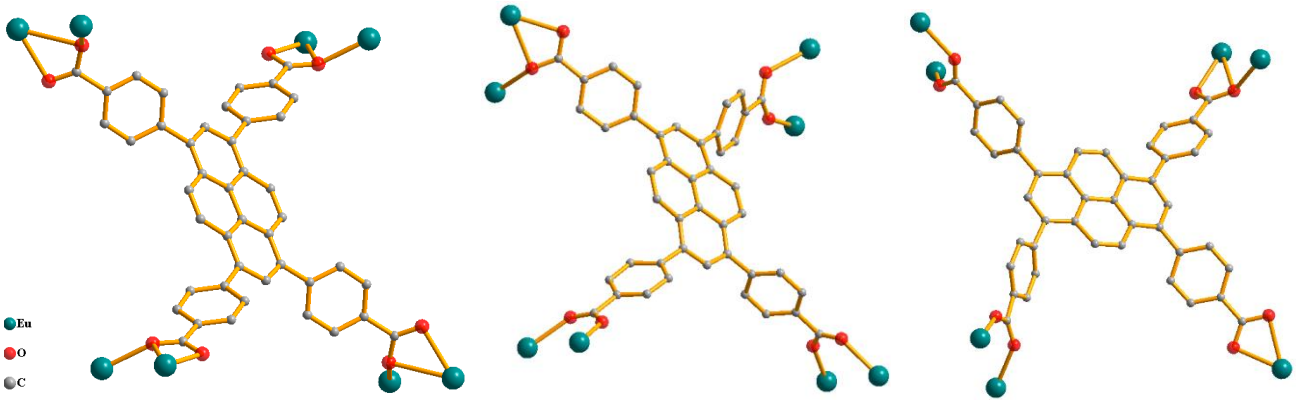

Figure S2. Schematic view of the coordination modes of the organic ligands in **JXNU-5**.

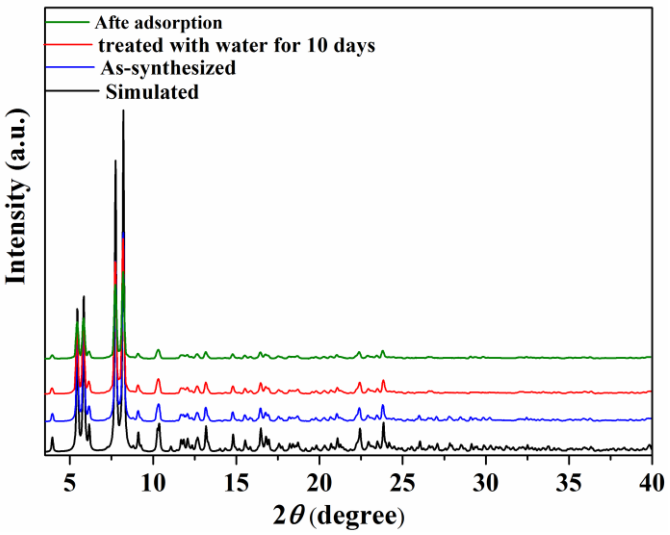

Figure S3. PXRD patterns for **JXNU-5**.

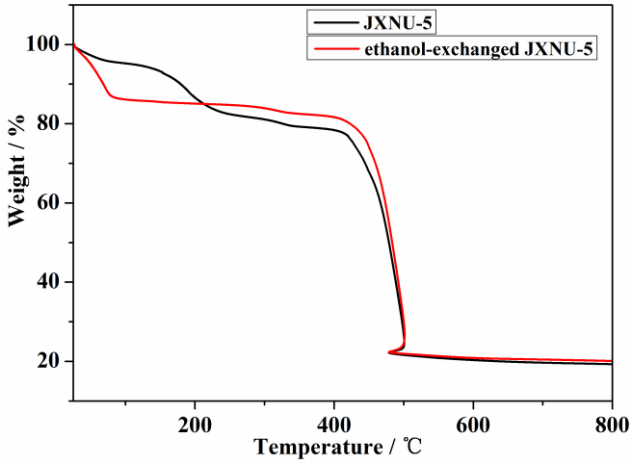

Figure S4. TGA curves.

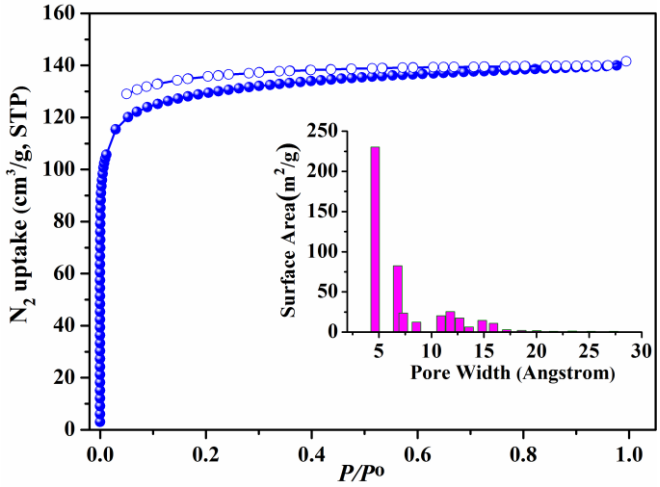

Figure S5. N_2 adsorption isotherm and pore-size distribution of **JXNU-5a**.

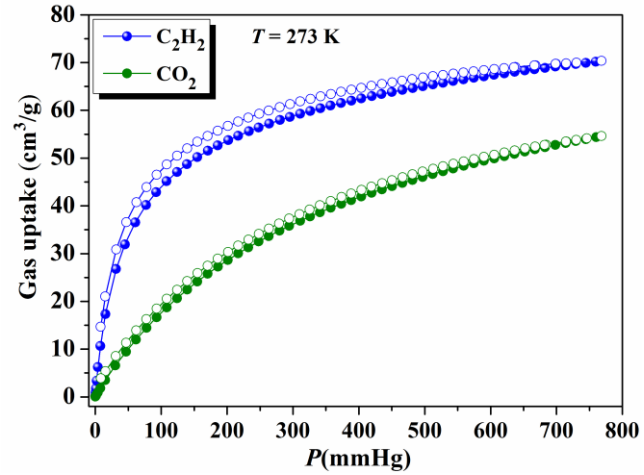

Figure S6. C_2H_2 and CO_2 adsorption isotherms of **JXNU-5a** at 273 K.(Adsorption and desorption branches are represented as closed and open symbols, respectively).

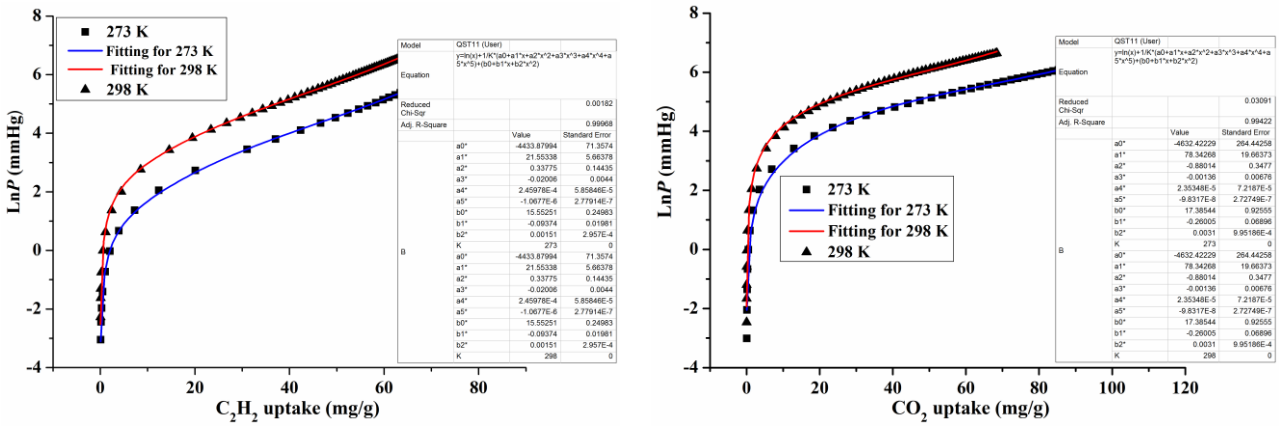

Figure S7. The Virial fits of C_2H_2 and CO_2 isortherms for **JXNU-5a**.

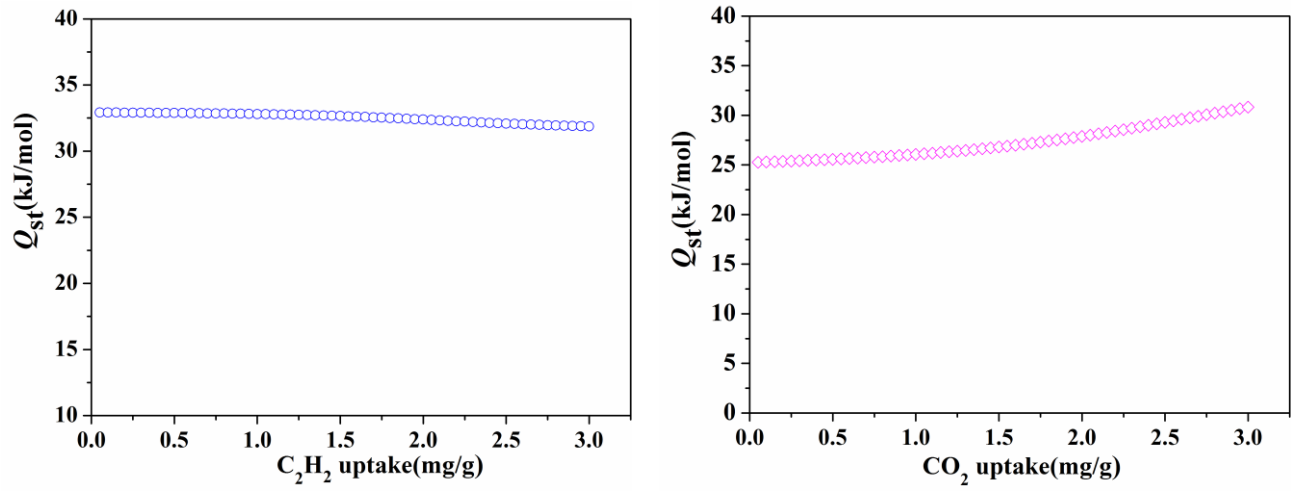

Figure S8. The Q_{st} of C_2H_2 and CO_2 adsorption for **JXNU-5a**.

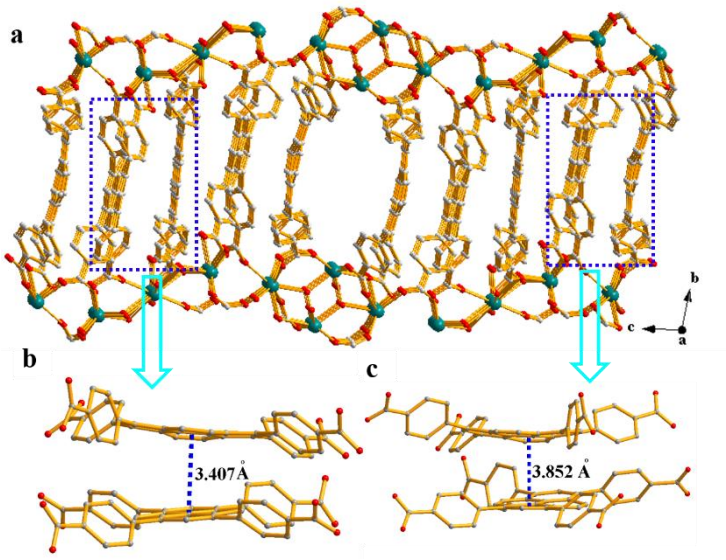

Figure S9. View of the π···π interactions in **JXNU-5**.

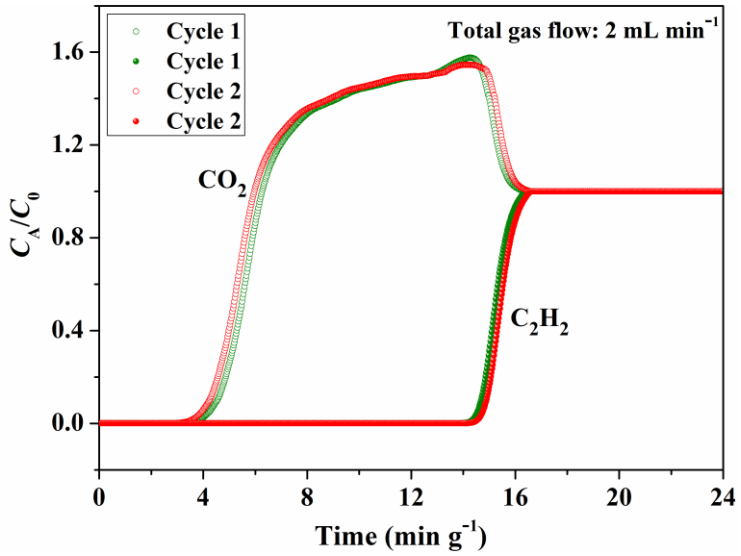

Figure S10. Cycling column breakthrough curves for C_2H_2/CO_2 separation (50/50, v/v) with J**XNU-5a** at 298 K and 1 atm.

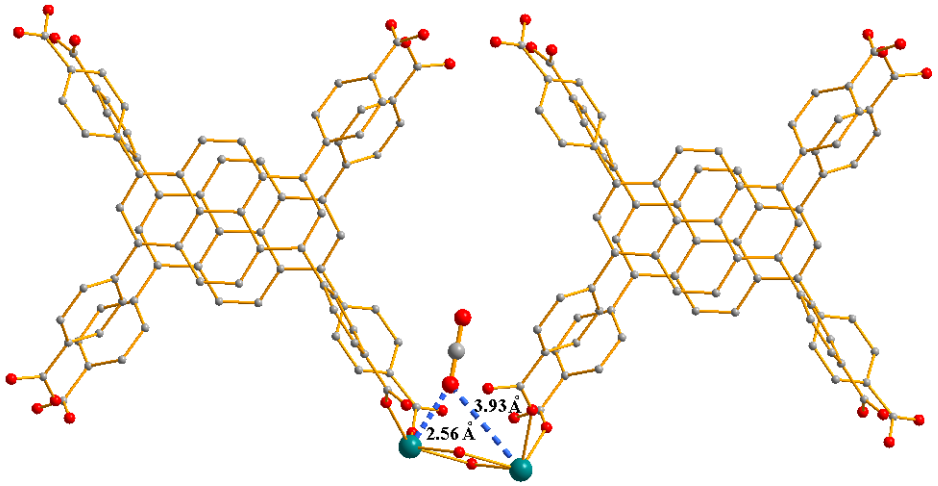

Figure S11. DFT-D-calculated the preferential binding sites for CO_2 adsorption in **JXNU-5a**.

Table S1. Selected Bond Lengths (Å) of **JXNU-5**.

Eu1−O4A [a]	2.353(5)	Eu2−O2	2.398(5)	Eu3−O15I	2.397(5)
Eu1−O4B	2.353(5)	Eu2−O3A	2.399(4)	Eu3−O13G	2.457(5)
Eu1−O20A	2.454(6)	Eu2−O6D	2.440(6)	Eu3−O14G	2.568(5)
Eu1−O20B	2.454(6)	Eu2−O19A	2.483(6)	Eu4−O21	2.322(4)
Eu1−O18	2.455(5)	Eu2−O1W	2.492(5)	Eu4−O10	2.326(6)
Eu1−O18C	2.455(5)	Eu2−O5D	2.528(5)	Eu4−O16L	2.335(6)
Eu1−O19A	2.784(7)	Eu2−O4A	2.894(5)	Eu4−O12J	2.349(6)
Eu1−O19B	2.784(7)	Eu3−O9	2.338(5)	Eu4−O21J	2.384(4)
Eu1−O17	2.821(5)	Eu3−O11H	2.343(5)	Eu4−O3W	2.441(6)
Eu1−O17C	2.821(5)	Eu3−O8E	2.345(5)	Eu4−O14K	2.450(5)
Eu2−O17	2.352(5)	Eu3−O1	2.353(4)	Eu4−O2W	2.465(7)
Eu2−O7E	2.373(4)	Eu3−O21	2.383(4)		

[a] symmetry Codes, A: $x-1, y, z$; B: $2-x, 1-y, 2-z$; C: $1-x, 1-y, 2-z$; D: $x-1, 1+y, z$; E: $x, 1+y, z$;F: $2-x, 2-y, 2-z$; G: $1+x, y-1, z$; H: $1+x, y, z$; I: $x, y-1, z$; J: $1-x, 1-y, 1-z$; K: $-x, 2-y, 1-z$; L: $1-x, 2-y, 1-z$.

Table S2. Dual-site Langmuir fit parameters for C_2H_2, and CO_2 in **JXNU-5a**.

	$q_{A,sat}$ mol kg^{-1}	b_{A0} Pa^{-1}	$q_{B,sat}$ mol kg^{-1}	b_{B0} Pa^{-1}
C_2H_2	1.7	1.64E-11	2.1	1.28E-10
CO_2	1.5	1.09E-12	2.5	6.22E-10

References

(1) Myers, A.-L.; Prausnitz, J. M. Thermodynamics of mixed-gas adsorption. *AIChE J.* **1965**, *11*, 121−127.

(2) Rowsell, J. L. C.; Yaghi, O. M. Effects of Functionalization, Catenation, and Variation of the Metal Oxide and Organic Linking Units on the Low-Pressure Hydrogen Adsorption Properties of Metal−Organic Frameworks. *J. Am. Chem. Soc*. **2006**, *128*, 1304−1315.

(3) Krishna, R.; Baur, R. Modelling Issues in Zeolite Based Separation Processes. *Sep. Purif. Technol.* **2003**, *33*, 213–254.

(4) Krishna, R. Screening Metal-Organic Frameworks for Mixture Separations in Fixed-Bed Adsorbers using a Combined Selectivity/Capacity Metric. *RSC Adv.* **2017**, *7*, 35724–35737.

(5) Liu, J.; Tian, J.; Thallapally, P. K.; McGrail, B. P. Selective CO_2 Capture from Flue Gas Using Metal-Organic Frameworks-A Fixed Bed Study. *J. Phys. Chem. C* **2012**, *116*, 9575–9581.